Tailoring thermochromic and optical properties of VO2 thin films by pulsed laser deposition using different starting routes

Yannick Bleu, Florent Bourquard, Damien Jamon, Anne-Sophie Loir, Florence Garrelie, Christophe Donnet

Version of Record: https://www.sciencedirect.com/science/article/pii/S0925346722010412
Manuscript_43b66a483b5f858875df7d9be62f0960

Tailoring thermochromic and optical properties of VO_2 thin films by pulsed laser deposition using different starting routes

Yannick Bleu, Florent Bourquard, Damien Jamon, Anne-Sophie Loir, Florence Garrelie, Christophe Donnet

Université de Lyon, Université Jean Monnet-Saint-Étienne, CNRS, Institut d'Optique Graduate School, Laboratoire Hubert Curien, UMR 5516, F-42023 Saint-Étienne, France

Abstract

The insulator to metal transition (IMT) of vanadium dioxide (VO_2) at about 68 ºC enables a variety of optical applications, including switching and modulation, and tuning of optical resonators. However, due to the multivalent nature of vanadium, controlling the synthesis of stoichiometric VO_2 is still a challenge. Moreoever, the temperature dependent optical properties are strongly influenced by the microstructure of the VO_2 thin film. In this paper, we report for the first time the effect on the microstructure and optical properties of two different routes implemented using the same PLD process to obtain VO_2 thin films exhibiting an IMT; one route involving ablation of a metallic vanadium (V) target in an oxygen atmosphere, the other ablation of a vanadium oxide V_2O_5 target in a vacuum, both followed by a similar rapid thermal annealing process. Each route leads to significantly different VO_2 thin films, exhibiting an IMT transition temperature of 69 °C with the V_2O_5 route, and of 50°C with the $V+O_2$ route. In addition, VO_2 films obtained from $V+O_2$ have a narrower hysteresis width, a smoother surface with very low roughness, a slightly higher refractive index, a higher absorption coefficient, and a narrower optical band gap than VO_2 film obtained from V_2O_5. The thermochromic and optical properties of both VO_2 are discussed in relation with the nanostructural properties. Our findings highlight the value and versatility of the PLD process in adapting the optical properties of VO_2 films to the application concerned.

1. Introduction

Vanadium dioxide (VO_2) thin films have been of great interest to researchers as they undergo an insulator to metal transition (IMT) at 68 °C. Upon heating, a reversible first order phase transition occurs from the monoclinic to the tetragonal phase involving a decrease in transmittance in the infrared region and electrical resistivity that can be of a few orders in

magnitude **[1,2]**. Thanks to this transition, many works have been devoted to studying the potential applications of VO_2, for example, Mott transistors**[3]**, smart window coatings**[4]**, ultra-fast switches and micro bolometers**[5]**, and optical resonant switches **[6]**. Indeed, pure VO_2 thin film is necessary to obtain a sharp and large hysteresis around 68 °C, and a synthesis of phase. However, achieving the synthesis of the pure VO_2 phase is still a challenge as vanadium has multiple oxidation states. Several methods of obtaining pure VO_2 thin film are reported in the literature, including chemical vapor deposition (CVD)**[7]**, sputtering**[8–12]**, solution based techniques**[13–15]** and pulsed laser deposition (PLD)**[16–18]**. Among these methods, VO_2 thin films have long been produced using PLD with a variety of target materials, oxygen gas pressures, laser energies, and other process parameters. Perhaps one of the most intriguing parameters is the target material itself. Several authors have reported on VO_2 thin film deposition using PLD using vanadium metal**[19]**, V_2O_5 **[20]**, V_2O_3**[2]** and VO_2 **[21]** as a target material. Among them, V_2O_5 and pure vanadium metal are the most frequently used. However, no recent reports compare the optical properties of VO_2 thin film obtained using these two vanadium-based targets with the same process. In 1997, Bowman et al.**[22]** reported the growth of VO_2 using PLD with both targets, and emphasized the effect of the applied strain on the resistance electrical resistivity of the resulting VO_2, but a systematic comparison of the thermochromic and optical properties of VO_2 thin films obtained using PLD from vanadium metal and V_2O_5 ceramic is still lacking.

In this paper, we report the synthesis and the optical properties of VO_2 thin films grown by pulsed laser deposition of vanadium metallic and V_2O_5 ceramic targets, both followed by rapid thermal annealing. Oxygen pressure was introduced during ablation of vanadium, to ensure the formation of vanadium oxide. The rapid thermal annealing process enables precise control of the crystallization of the grown films, with minimum diffusion of impurities from the glass substrate into the films that can be detrimental for the thermochromic properties. We report the results of our investigation of the nanocrystalline structure and morphology of thermochromic properties such as the transmittance commutation from insulating to the metallic phase, the transition temperature, the hysteresis width, and other optical properties including absorbance in the visible ranges, the optical energy gap (E_g) and optical conductivity of VO_2 films obtained from both targets. Using the deposited thin films from both targets with the same post annealing process resulted in two VO_2 thin films with different nanostructural and optical properties. Understanding the dependence of any starting

ablated materials on the VO_2 properties can thus help to stabilize VO_2 synthesis with the functional properties desired.

2. Experimental details

Deposition and annealing of the VO_2 *films*

The synthesis route of VO_2 is a two-step process, as depicted in Fig.1. Prior to deposition, the SiO_2 substrates were cleaned using a three-step cleaning process in acetone, ethanol, and deionized water baths for 30 min each.

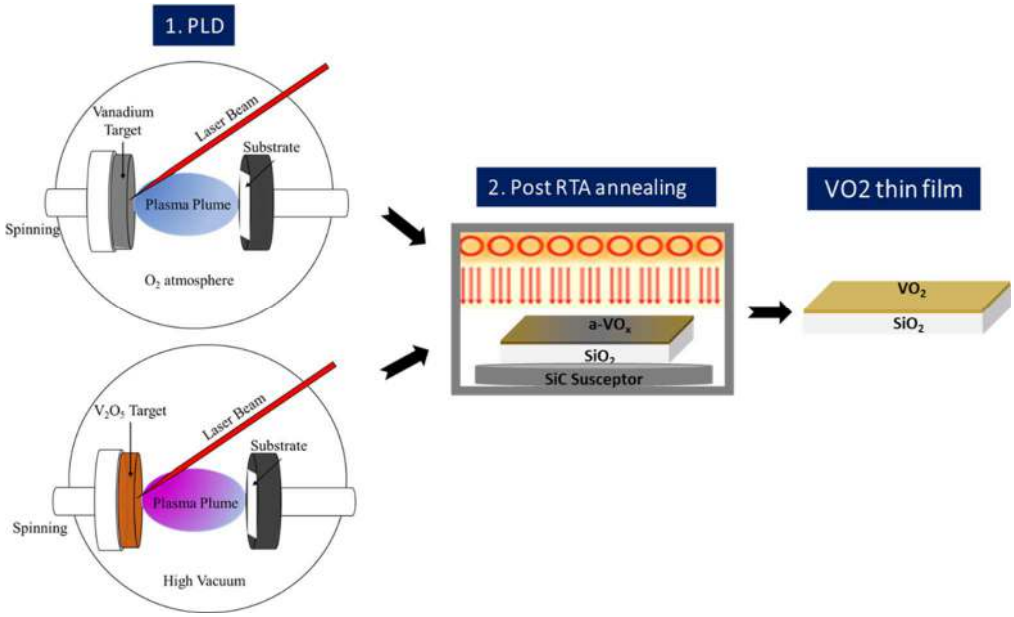

Figure 1: Synthesis steps for VO_2 films obtained by pulsed laser deposition and rapid thermal annealing on SiO_2.

The first step was the pulsed laser deposition of the target materials. The PLD chamber was evacuated to a background pressure of 1.7×10^{-7} mbar. Two types of targets were used in the investigation: pure metallic vanadium (V) and ceramic V_2O_5 targets, both with a purity of 99.9%. A KrF excimer laser operating at 248 nm and 10 Hz with a fluence of 13 J/cm^2 was used to ablate the targets. The distance between the target and the substrate was set at 5 cm and the laser beam was placed at an angle of 45° to the target. For the metallic vanadium, the oxygen pressure was 1×10^{-2} mbar (1 Pa) inside the deposition chamber using ultrapure O_2. The ablation of the V_2O_5 target was performed without oxygen gas. The substrates were maintained at room temperature and the targets were rotated during the deposition process to ensure uniform ablation of its surface. For both depositions, the average deposition rate was measured using profilometry. The deposition rate for V+O_2 was around 3 nm/min, while the

rate for V_2O_5 was 6 nm/min. The deposition time was then adjusted to obtain 100 nm thin films.

The second step was the rapid thermal annealing process on the as-deposited VO_x films using a RTP machine (AS-One RTP system from Annealsys, France). This step consisted in heating the samples at 400 °C for 600 s at an oxygen partial pressure of 1 mbar (1 Pa) and a 50 sccm flow, with a heating rate of 5 °C/s and natural cooling. The annealing chamber was evacuated to a 1×10^{-2} mbar pressure before the oxygen was introduced. These conditions were the result of several preliminary optimizations to obtain the best thermochromic behavior of the deposited films. It is worth mentioning that for technical convenience, the VO_2 samples were grown on two different substrates: SiO_2 for Raman and transmittance measurements, Si for ellipsometry, GIXRD, AFM and SEM analysis.

Characterization

The VO_2 thin films were characterized in terms of the surface morphology, micro-structure and optical properties. Raman analysis (Jobin-Yvon ARAMIS) was performed using a 633 nm excitation wavelength, with a laser power of 0.1 mW and a laser beam was focused with a 100x objective, consistent with a laser spot diameter of less than 1 mm. Ellipsometry (HORIBA Jobin Yvon UVISEL) was performed using a heated sample holder whose temperature was controlled by a thermocouple between 15 and 85 °C. The experimental ellipsometric parameters were fitted with a Tauc-Lorentz formula using three oscillators. Scanning electron microscopy (SEM) (JEOL IT 800 SHL) and atomic force microscopy (AFM) (Icon BRUKER) were used to analyze the morphology and roughness of the films. Grazing-incidence X-ray diffraction (GIXRD) was performed on an AERIS diffractometer (MALVERN PANALYTICAL) with a CuKα X-ray source (0.1542 nm) of 450W. Data were collected in a 2θ configuration with an incidence angle $\omega = 0.4°$, a 2θ acquisition range from 20° to 75° and a step size of 0.04°. The VO_2 crystallite size D was quantified by the Scherrer equation $D = (0.89.\lambda / \beta.\cos\theta)$ **[23]** with λ the X-ray wavelength, β and θ respectively the FWHM and diffraction angle of the diffraction peak of VO_2, using the instrumental peak width deduced from a referenced LaB_6 powder whose diffractogram was recorded in similar conditions to those used for the VO_2 films. Considering the diffraction patterns obtained, D was calculated as the average value deduced from the four most intense diffraction peaks within the range 25° to 60°. UV–Visible spectroscopy was performed in absorbance mode

within the spectral range 200–900 nm at room temperature. The thermochromic properties of the films were measured by collecting the transmittance between 20-100 °C in the visible and IR wavelength ranges using a fiber optic spectrometer equipped with handmade heating units. For all samples, the integrated luminous transmittance (T_{lum}, 380–780 nm) and solar modulation efficiency (T_{sol}, 300–2500 nm) were calculated from the following equation:

$$T_{lum,sol} = \frac{\int \varphi_{lum,sol}(\lambda) T(\lambda) d\lambda}{\int \varphi_{lum,sol}(\lambda) d\lambda} \qquad (1)$$

where $T(\lambda)$ denotes film transmittance at wavelength (λ), $\varphi_{lum}(\lambda)$ is the standard luminous efficiency function for the photopic vision of human eye, $\varphi_{sol}(\lambda)$ is the solar irradiance spectrum for air mass 1.5 corresponding to the sun at an angle of 37° to the horizon**[24]**. ΔT_{sol} is obtained from : $\Delta T_{sol} = T_{sol}(20\ °C) - T_{sol}(90\ °C)$ and $T_{lum} = ½(T_{lum}(20\ °C) + T_{lum}(90\ °C))$.

3. Results and discussion

a. Crystalline structure and surface morphology

Prior to RTA treatments, the as-deposited films a-VO_x films were analyzed using Raman spectroscopy, as depicted in Fig. 2. According to **[25,26]**, the Raman spectrum of a-VO_x film obtained from the V_2O_5 target is dominated by scattering on vanadyl bonds (V═O) centered around 840 cm^{-1} (Fig. 2a). It also has another weaker broad feature centered around 400 cm^{-1} originating from different complex atomic vibrations. This band is also observed with a very similar feature, on the Raman spectrum of the VO_x film obtained from the V target with O_2 gas. This film also has a rather low intensity band centered at 705 cm^{-1} with the same origin as the band centered at 840 cm^{-1}. Indeed, according to these authors, the shift in this band can be attributed to oxygen deficiency in the VO_x lattice: a lower wavenumber is attributed to an increase in oxygen deficiency. We can therefore state that the as-deposited a-VO_x from the V target with O_2 gas may contain less oxygen than a-VO_x deposited using V_2O_5 target.

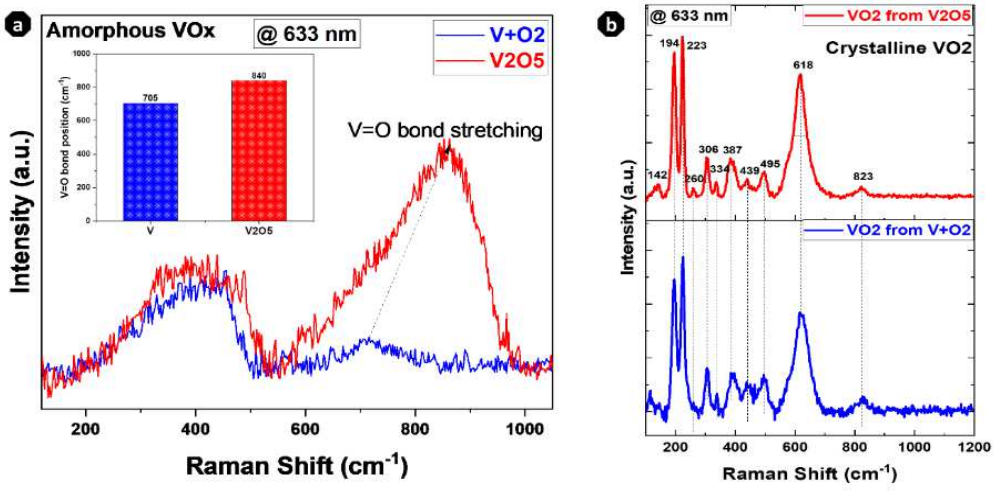

Figure 2: Room-temperature Raman spectra: (a) Raman spectra a-VO_x samples from both targets: V+O_2 in blue and V_2O_5 in red; the insert is a bar plot of the position of vanadyl V=O bond for each a-VO_x deposit; (b) Raman spectra crystalline VO_2 samples from both targets: V+O_2 in blue and V_2O_5 in red, both after RTA.

Next, after rapid thermal annealing to crystallize both a-VO_x into a VO_2 phase, Raman spectroscopy was used to check the presence of the monoclinic VO_2 room temperature phase. The narrow peaks in the Raman spectra in Fig. 2b confirm high crystalline quality with the typical Raman signature of monoclinic VO_2 in both kinds of thin film. Indeed, among the 18 Raman-active phonon modes predicted by group theory analysis for all low-temperature phase symmetries of VO_2, we observed 11 vibrational modes. These different vibrational modes at 142, 194(Ag), 223(Ag), 260(Bg), 306(Ag/Bg), 334(Bg/ Ag), 387(Ag), 439(Bg), 495(Ag), 618(Ag), 823(Bg) cm^{-1} are characteristic of pure VO_2(M1) phase**[27,28]**. Lower wavenumber phonon modes at 193 and 223 cm^{-1} were attributed to V-V vibrations, while the 618 cm^{-1} peak corresponds to the stretching mode of V-O bonds**[29]**. No Raman shifts were identified for other kinds of vanadium oxides or any other types of polymorphs of VO_2 (M2/T)**[30]**. The peak located around 620 cm^{-1} is the most structure-sensitive position for VO_2. Recently, Maklakov et al.**[31]** used the FWHM of this peak to discuss the crystallinity of VO_2. Indeed, the width of a Raman band of a nanocrystalline material is known to decrease with an increase in the size of the crystal, or the defect concentration decreases. A reduction in the Raman linewidth may also be caused by the increasingly uniform size of the nanocrystals **[32,33]**. Likewise, in our case, the FWHM of the V-O peak located at 618 cm^{-1} for VO_2 from V+O_2 was about 45 cm^{-1}, while the one for VO_2 obtained from V_2O_5 was about 54 cm^{-1}. This probably means that the VO_2 obtained using V_2O_5 has either a larger nanocrystalline grain size with fewer defects, or more uniform nanocrystal size than the VO_2 prepared using V+O_2. This observation was corroborated by the GIXRD and SEM analyses presented next.

Fig. 3 shows the typical GIXRD patterns of the two VO_2 films. According to the ICDD card N°04-003-2035 (COD data base), the peaks detected in both samples can be attributed to a VO_2 monoclinic M1 phase. However, we observed few traces of V_2O_3. Most of the peaks were intense and narrow, suggesting that the samples were well crystallized. The (200) peak

dominated the XRD patterns of both VO_2 thin films, indicating a preferred orientation in the (200) direction whatever the synthesis route. Several minor orientations appeared in the patterns, a qualitative indication that both VO_2 were textured. In addition, the average grain sizes deduced from the Scherrer equation of VO_2 films obtained from $V+O_2$ and V_2O_5 were estimated to be 14 and 42 nm, respectively.

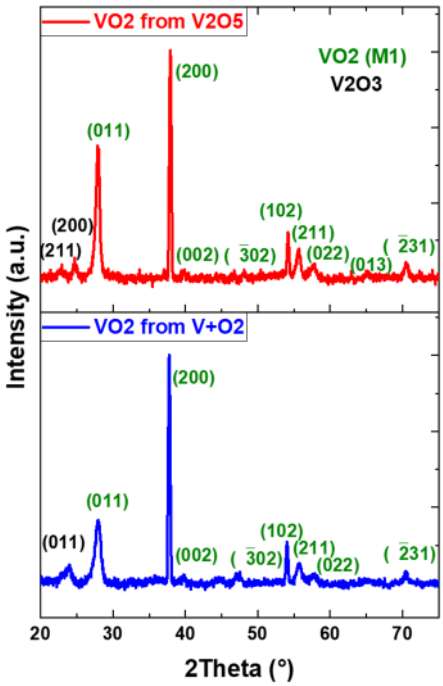

Figure 3: Room-temperature GIXRD patterns: VO_2 films obtained from $V+O_2$ are shown in blue and those obtained from V_2O_5 in red.

Fig. 4 shows SEM and AFM images of the surface morphologies of the two VO_2 thin films. The VO_2 obtained from $V+O_2$ has a smooth surface with only 0.8 nm of roughness (Fig. 4a) with no visible grains, probably because they are too small to be visible, as noted above using GIXRD grain size estimation. Whereas the VO_2 obtained from V_2O_5 represented the average grain size of around 80 nm, probably inducing the higher surface roughness of 5 nm (Fig. 4b). Indeed, grain size estimated using SEM image processing with ImageJ software was double that estimated using the Scherrer equation in GIXRD. This discrepancy may be due to the processing limit. However, both analyses confirmed that the VO_2 film obtained from $V+O_2$ has smaller grains than the film obtained from V_2O_5. Nevertheless, the roughness of both the films was similar to that of the typical sputtering of VO_2 films obtained by PLD**[34,35]**. It is also worth noting that the VO_2 film obtained from V_2O_5 was porous whereas the film obtained

from $V+O_2$ showed no porosity at our observation scale. Moreover, the thickness of both VO_2 films observed in cross-section SEM analysis was 36-40 nm. This means that the initial film thickness of 100 nm decreased after rapid thermal annealing due to the densification and crystalization of the films. The decrease in thickness was confirmed by ellipsometry, as described next.

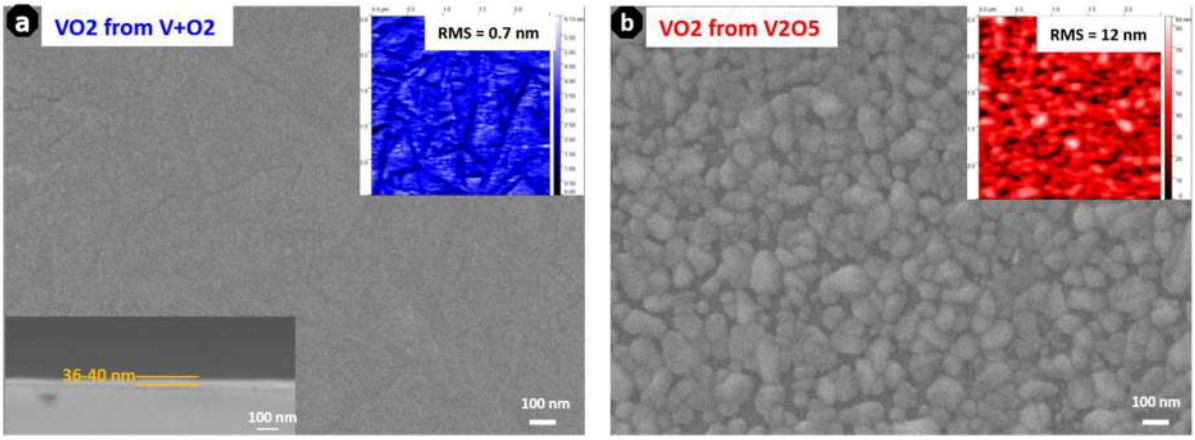

Figure 4: Top-view SEM micrographs of VO_2 thin films: (a) SEM image of VO_2 deposited from $V+O_2$, the top blue insert corresponds to the AFM image showing the smooth surface of this thin film, the insert at the bottom left is the cross-section SEM image showing the VO_2 thickness of 36 to 40 nm. (b) SEM image of VO_2 deposited from V_2O_5, the top red insert corresponds to the AFM image showing a rougher surface. Scale bar = 100 nm.

b. Thermochromic and optical properties

To assess the characteristic IMT of grown VO_2 thin films, we measured their transmittance as a function of temperature. Fig. 5a-b illustrate the hysteresis loop at 1550 nm obtained from the optical transmittance Tr of each sample as a function of temperature, and a plot of d(Tr)/d(T). As shown in Fig. 5a, both VO_2 thin films underwent semiconductor IMT when heated from room temperature to higher temperatures, and vice versa. The VO_2 obtained from V_2O_5 underwent a sharper and more abrupt change in transmittance than the VO_2 obtained from $V+O_2$. The IMT parameters of both VO_2 thin films were determined by using the first derivative of the transmittance with respect to temperature. The phase transition temperature T_t is expressed as the average transition temperature between the transition temperatures observed during heating (T_h) and cooling (T_c), ($T_t = 1/2 (T_h + T_c)$), while the thermal

hysteresis width ΔT is defined as the absolute difference in temperature between T_h and T_c cycle transition, ($\Delta T = (T_h - T_c)$). The VO_2 deposited from V_2O_5 showed a higher IMT temperature (T_t) (69 °C) with a larger hysteresis width of 11 °C. In contrast, the VO_2 obtained from $V+O_2$ showed a reduced T_t of 50 °C with a narrower hysteresis of 6 °C, as shown in Fig.5c. According to previous reports in the literature**[36,37]**, the oxygen vacancies reduced the critical temperature. Since the ablation of $V+O_2$ results in amorphous VO_x with lower oxygen content than its counterpart obtained from V_2O_5, following the same post annealing process to crystallize them, the VO_2 obtained from $V+O_2$ probably kept less oxygen, resulting in VO_2 film with oxygen. This may explain the distinct difference in the transition temperature for the two VO_2 films.

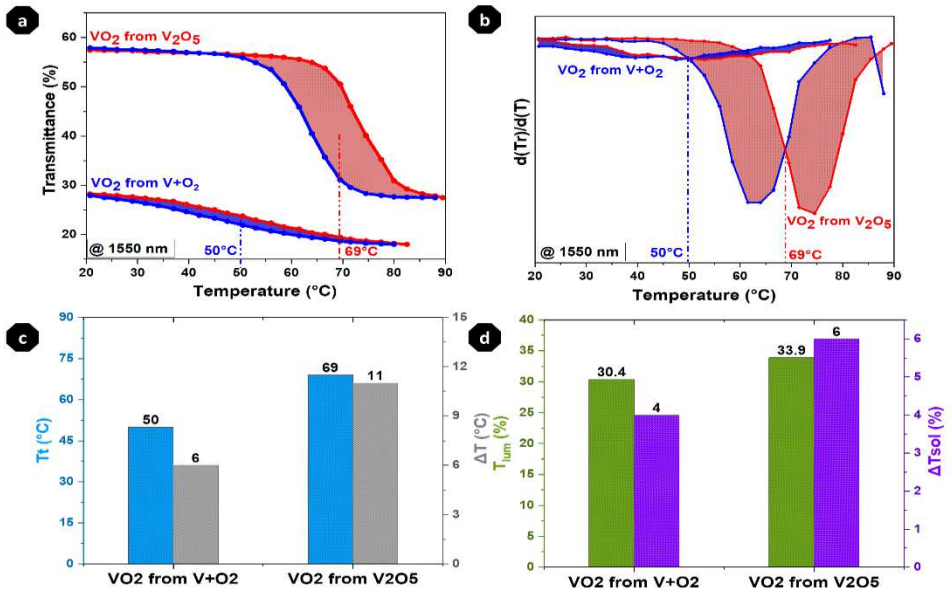

Figure 5: (a) hysteresis loops at 1550 nm, (b) the corresponding d(Tr)/d(T)&T curve for both VO_2 thin films, (c) the phase transition temperature and the hysteresis width for both VO_2 films, (d) The calculated optical performance T_{lum} and ΔT_{sol}.

The calculated optical performances (T_{lum} and ΔT_{sol}) are plotted in Fig. 5d. The average luminous transmittance was 33.9% for VO_2 obtained from V_2O_5, which is slightly higher than the luminous transmittance of the VO_2 film obtained from $V+O_2$, which was 30.4%. This means that the VO_2 film obtained from V_2O_5 was slightly more transparent in the visible range than the other VO_2 film. This observation was confirmed by the absorbance measurement of both films. The solar modulation efficiency of the VO_2 film obtained using V_2O_5 was also higher than that of the VO_2 film obtained from $V + O_2$ gas.

Further, the VO_2 crystallite size and its distribution are assumed to determine the width and shape of the heating-cooling hysteresis loop, whereas the temperature depends on transmittance. More precisely, it has been shown that a high-quality VO_2 crystal and narrow crystallite size distribution resulted in a narrow hysteresis loop and vice versa**[38]**. However, it has also been shown that the increase in the size of the crystallite due to recrystallization also increased the width of the hysteresis loop**[39]**. In the present study, the VO_2 film obtained from V_2O_5 had a bigger hysteresis loop with larger grain size and higher roughness than the VO_2 film obtained from $V+O_2$ which had a smaller hysteresis loop with lower roughness and probably smaller grain size. Our results are thus consistent with those of the abovementioned studies.

To go futher in the optical investigation of synthetized vanadium dioxide, temperature controlled ellipsometry measurements were made of both VO_2 films to obtain the n and k, which respectively represent the refraction ability of the material to incidence light, and the extinction coefficient, indicating the absorption of light. Fig. 6 shows the wavelength dispersions of the refractive index n and the extinction coefficient k of both VO_2 thin films, below (25 °C) and above (85 °C) their transition temperatures. It is clear that both the n or k values are temperature-independent in the visible spectrum, whereas the switching behavior is highly accentuated in the near-infrared region. This significant switching of the optical constants of both VO_2 presents a similar trend as the one reported recently by Zhang et al.**[40]**. It also confirms the good thermochromic properties of both VO_2.

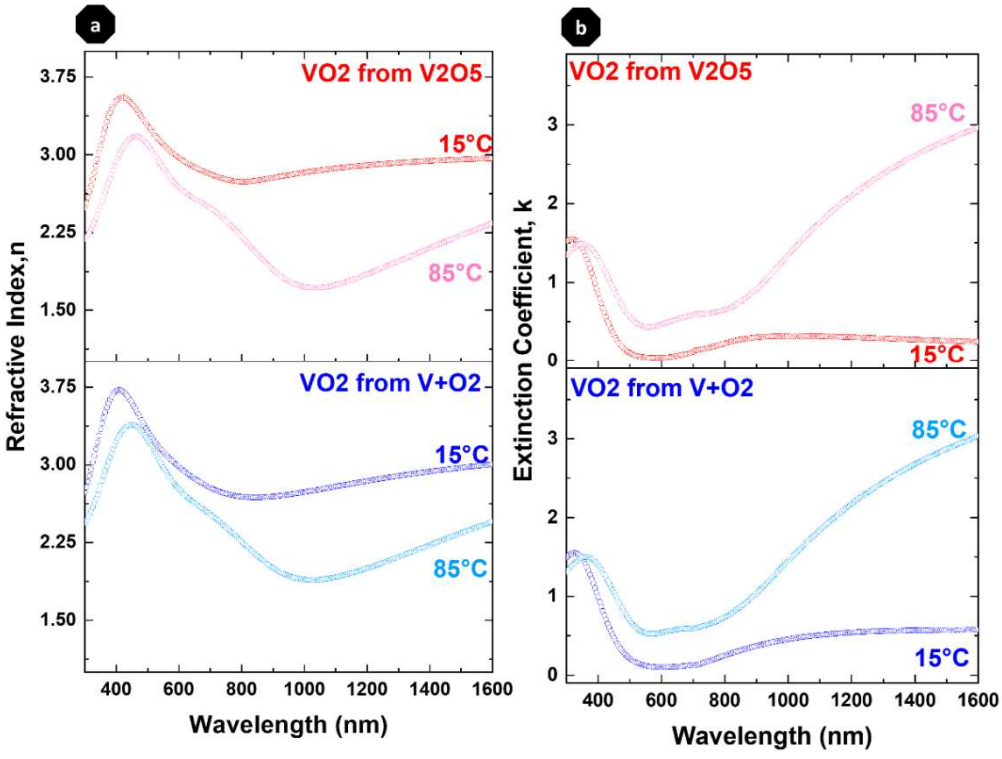

Figure 6. (a) Refractive index, n and (b) extinction coefficient, k of both VO_2 thin films at temperatures below and above the phase transition temperature determined by spectroscopic ellipsometry.

To better observe the difference in the n and k values of the two VO_2 films, we extracted the values at two specific wavelengths in the visible and IR ranges (see results in Table 1). We observed that the VO_2 obtained from $V+O_2$ presented slightly higher values of n and k in both the visible and IR regions. The higher values of k in the VO_2 film obtained from $V+O_2$ indicates that this VO_2 absorbs more than its counterpart obtained from V_2O_5. It is worth mentioning that the values of n and k we obtained in our experiment are in good agreement with those reported in the literature for films obtained using other deposition processes **[13,40,41].**

	VO_2 from $V+O_2$		**VO_2 from V_2O_5**		**VO_2 from $V+O_2$**		**VO_2 from V_2O_5**	
	n15 °C	n85 °C	n15 °C	n85 °C	k15 °C	k85 °C	k15 °C	k85 °C
550 nm (most sensitive for human eyes)	3.124	2.976	3.099	2.874	0.119	0.532	0.047	0.434
1550 nm (Infrared)	2.989	2.399	2.961	2.283	0.574	2.956	0.250	2.888

Table 1: Extracted values of n and k at specific wavelengths (550, and 1550 nm) for both VO_2 films.

In addition, in the optical constant spectra, at a wavelength of 1000 nm, n decreased and increased strongly with the rise and drop in temperature, and k increased and decreased respectively. A similar trend has been observed by others **[40,42,43]**. It was proven by Nagashima et al.**[44]** that the switching of n and k of VO_2 thin films depends to a large extent on the growing conditions. The optical constant hysteresis behaves in a similar way to the optical transmittance/absorbance hysteresis of VO_2 thin films. The hysteresis width of about 11 °C and the refractive index with an abrupt variation of n at 69 °C is similar to that obtained in optical transmittance of polycrystalline sputtered VO_2 thin films**[45]**. The extinction coefficient k also displays excellent phase transition characteristics but only in the near-infrared region.

Absorbance was measured at room temperature in the 300-900 nm range from which the optical band gap and the optical conductivity were deduced. Fig. 7a shows the absorbance measurements for both VO_2 thin films. The results clearly reveal the change in the absorption edge toward the blue region. The absorbance of the VO_2 obtained from $V+O_2$ was higher than that of the VO_2 obtained from V_2O_5. This observation corrobated the fact that this sample had a higher extinction coefficient and lower T_{lum}.

The optical band gap was evaluated from the absorption edge of the UV-Vis spectra. The indirect optical band gap was estimated using the Tauc plot:

$$(\alpha h\nu)^{1/2} \propto \left(E - E_g\right) \quad (2)$$

and the optical absorption coefficient α was calculated from the optical absorbance A using the relation**[46]**:

$$\alpha h\nu = \frac{2.303\ A}{X} \quad (3)$$

where X is the sample thickness in cm, α is the absorption coefficient and E_g is the optical band gap energy. The E_g value is extrapolated by the linear portion of the plot to $(\alpha h\nu)^{1/2} = 0$.

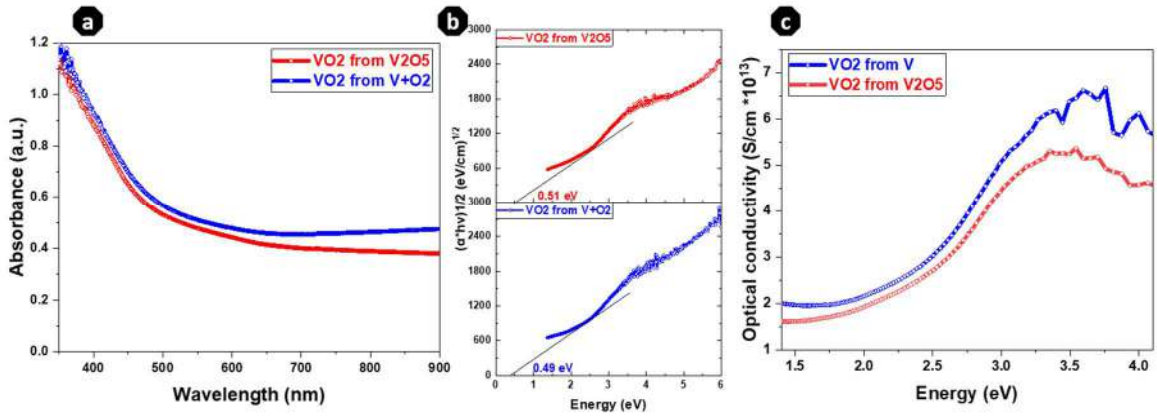

Figure 7. (a) Absorption spectra; (b) Plot of $(\alpha h\nu)^{1/2}$ versus photon energy ($h\nu$); (c) Variation in optical conductivity as a function of photon energy for both VO_2 thin films.

The optical band gap (0.51 eV) of the VO_2 film obtained from V_2O_5 was slighty higher than the value (0.49 eV) of the VO_2 film obtained from $V+O_2$ (Fig. 7b). These values are consistent with recent work on VO_2 film fabricated with V metallic target in argon and oxygen atmosphere using magnetron sputtering reported by Zhang et al.**[40]**. Indeed, according to previous work, the widening of the optical band gap induces a blue shift and an

enhanced visible transmittance**[47]**. This can explain the higher visible transmittance of the VO_2 obtained from V_2O_5.

Using the absorption coefficient (α) and refractive index (n) of the material, it is possible to calculate the optical responses of a material in terms of optical conductivity σ_{opt}, which is given by the relation**[48]** :

$$\sigma_{opt} = \frac{\alpha\, n\, C}{4\,\pi} \quad (4)$$

where C is the velocity of light.

Fig. 7c shows the variation in the optical conductivity as a function of photon energy for both VO_2 thin films. We observed that the optical conductivity increased with an increase in photon energy. As the VO_2 film deposited from $V+O_2$ had a higher absorption coefficient and refractive index, logically, it had higher optical conductivity than the VO_2 film obtained from V_2O_5. Our results therefore suggest that the optical conductivity of the obtained VO_2 films follows the same trend as the absorption coefficient and refractive index with increasing wavelength.

4. Conclusion

In this work, we demonstrated that the pulsed laser deposition of both vanadium metallic (in the presence of an O_2 atmosphere) and V_2O_5 ceramic targets, combined with post-rapid thermal annealing, result in the growth of two VO_2 thin films with different nanostructural and optical properties.

- The VO_2 obtained from the pulsed laser deposition of $V+O_2$ exhibits smaller nanocrystalline grain size with more defects and a smoother surface than the film obtained from V_2O_5.
- The VO_2 deposited from $V+O_2$ shows a lower IMT transition temperature of around 50 °C with a narrower hysteresis of 6 °C and slightly lower solar modulation efficiency with low visible transmittance than the VO_2 obtained from V_2O_5. Th reduced T_t value is probably due to the oxygen deficiency in the VO_2 prepared using the PLD of $V+O_2$.

- The VO_2 deposited from $V+O_2$ has a higher absorption coefficient and refractive index, with a slighty lower optical band gap and higher optical conductivity than the VO_2 obtained from V_2O_5.

This work highlighted the fact that the thermochromic and optical properties of VO_2 thin film also depends on the target materials. These results provide useful information to define a robust method for adjusting an important PLD parameter such as the target materials to use to produce high quality VO_2 thin films.

Acknowledgments

This work was supported by the LABEX MANUTECH-SISE (ANR-10-LABX-0075) of University of Lyon, in the program "*Investissements d'Avenir*" (ANR-11-IDEX-0007) run by the French National Research Agency (ANR).

References

[1] J.-H. Yu, S.-H. Nam, J.W. Lee, J.-H. Boo, Enhanced Visible Transmittance of Thermochromic VO2 Thin Films by SiO2 Passivation Layer and Their Optical Characterization, Materials. 9 (2016) 556. https://doi.org/10.3390/ma9070556.

[2] D.H. Kim, H.S. Kwok, Pulsed laser deposition of VO2 thin films, Appl. Phys. Lett. 65 (1994) 3188–3190. https://doi.org/10.1063/1.112476.

[3] S.A. Pauli, R. Herger, P.R. Willmott, E.U. Donev, J.Y. Suh, R.F. Haglund, X-ray diffraction studies of the growth of vanadium dioxide nanoparticles, Journal of Applied Physics. 102 (2007) 073527. https://doi.org/10.1063/1.2786917.

[4] Z. Zhang, Y. Gao, Z. Chen, J. Du, C. Cao, L. Kang, H. Luo, Thermochromic VO2 Thin Films: Solution-Based Processing, Improved Optical Properties, and Lowered Phase Transformation Temperature, Langmuir. 26 (2010) 10738–10744. https://doi.org/10.1021/la100515k.

[5] R.T. Rajendra Kumar, B. Karunagaran, D. Mangalaraj, Sa.K. Narayandass, P. Manoravi, M. Joseph, V. Gopal, Pulsed laser deposited vanadium oxide thin films for uncooled infrared detectors, Sensors and Actuators A: Physical. 107 (2003) 62–67. https://doi.org/10.1016/S0924-4247(03)00233-4.

[6] E.K. Koussi, I. Verrier, T. Kämpfe, S. Reynaud, F. Bourquard, D. Jamon, H. Bruhier, Y. Jourlin, O. Parriaux, Thermally activated resonant grating using a vanadium dioxide waveguide, Opt. Mater. Express, OME. 11 (2021) 1093–1103. https://doi.org/10.1364/OME.413373.

[7] M. B. Sahana, M. S. Dharmaprakash, S. A. Shivashankar, Microstructure and properties of VO 2 thin films deposited by MOCVD from vanadyl acetylacetonate, Journal of Materials Chemistry. 12 (2002) 333–338. https://doi.org/10.1039/B106563G.

[8] F. Guinneton, L. Sauques, J.C. Valmalette, F. Cros, J.R. Gavarri, Comparative study between nanocrystalline powder and thin film of vanadium dioxide VO2: electrical and infrared properties, Journal of Physics and Chemistry of Solids. 62 (2001) 1229–1238. https://doi.org/10.1016/S0022-3697(01)00013-0.
[9] H.Y. Xu, Y.H. Huang, S. Liu, K.W. Xu, F. Ma, P.K. Chu, Effects of annealing ambient on oxygen vacancies and phase transition temperature of VO2 thin films, RSC Adv. 6 (2016) 79383–79388. https://doi.org/10.1039/C6RA13189A.
[10] A. Dey, M.K. Nayak, M.S. Pradeepkumar, D. Porwal, B. Yougandar, A. Carmel Mary Esther, Studies on Mo doped vanadium oxide film by pulsed RF magnetron sputtering, Surface and Interface Analysis. 49 (2017) 805–808. https://doi.org/10.1002/sia.6226.
[11] A.M. Selman, M.J. Kadhim, Fabrication of high sensitivity and fast response IR photodetector based on VO2 nanocrystalline thin films prepared on the silicon substrate, Optical Materials. 131 (2022) 112664. https://doi.org/10.1016/j.optmat.2022.112664.
[12] Z. Xiang, Z. Wu, Y. Shi, C. Li, X. Chen, J. Gou, J. Wang, Y. Zhuang, X. Dong, X. Zheng, Y. Jiang, Optimized thermochromic properties for smart window application of VO2 films by wet-etching process, Optical Materials. 128 (2022) 112359. https://doi.org/10.1016/j.optmat.2022.112359.
[13] J. Zhang, J. Wang, C. Yang, H. Jia, X. Cui, S. Zhao, Y. Xu, Mesoporous SiO2/VO2 double-layer thermochromic coating with improved visible transmittance for smart window, Solar Energy Materials and Solar Cells. 162 (2017) 134–141. https://doi.org/10.1016/j.solmat.2016.12.048.
[14] Md.A. Rashid, B.K. Mondal, M.H.K. Rubel, Md.M. Rahman, O.T. Mefford, J. Hossain, Synthesis of Self-Assembled Randomly Oriented VO2 Nanowires on a Glass Substrate by a Spin Coating Method, Inorg. Chem. 59 (2020) 15707–15716. https://doi.org/10.1021/acs.inorgchem.0c02108.
[15] S. Guan, M. Gaudon, A. Rougier, E. Duguet, E. Durand, A. Fargues, O. Viraphong, N. Penin, VO2 films obtained by V2O5 nanoparticle suspension reduction, Optical Materials. 127 (2022) 112117. https://doi.org/10.1016/j.optmat.2022.112117.
[16] D. Bhardwaj, A. Goswami, A.M. Umarji, Synthesis of phase pure vanadium dioxide (VO2) thin film by reactive pulsed laser deposition, Journal of Applied Physics. 124 (2018) 135301. https://doi.org/10.1063/1.5046455.
[17] S.A. Bukhari, S. Kumar, P. Kumar, S.P. Gumfekar, H.-J. Chung, T. Thundat, A. Goswami, The effect of oxygen flow rate on metal–insulator transition (MIT) characteristics of vanadium dioxide (VO2) thin films by pulsed laser deposition (PLD), Applied Surface Science. 529 (2020) 146995. https://doi.org/10.1016/j.apsusc.2020.146995.
[18] E.-K. Koussi, F. Bourquard, T. Tite, D. Jamon, F. Garrelie, Y. Jourlin, Synthesis of vanadium oxides by pulsed laser deposition and rapid thermal annealing, Applied Surface Science. 521 (2020) 146267. https://doi.org/10.1016/j.apsusc.2020.146267.
[19] R. McGee, A. Goswami, B. Khorshidi, K. McGuire, K. Schofield, T. Thundat, Effect of process parameters on phase stability and metal-insulator transition of vanadium dioxide (VO2) thin films by pulsed laser deposition, Acta Materialia. 137 (2017) 12–21. https://doi.org/10.1016/j.actamat.2017.07.025.
[20] Y.X. Guo, Y.F. Liu, C.W. Zou, Z.M. Qi, Y.Y. Wang, Y.Q. Xu, X.L. Wang, F. Zhang, R. Zhou, Oxygen pressure induced structure, morphology and phase-transition for VO2/c-sapphire films by PLD, Appl. Phys. A. 115 (2014) 1245–1250. https://doi.org/10.1007/s00339-013-7972-0.
[21] L.L. Fan, Y.F. Wu, C. Si, C.W. Zou, Z.M. Qi, L.B. Li, G.Q. Pan, Z.Y. Wu, Oxygen pressure dependent VO2 crystal film preparation and the interfacial epitaxial growth

study, Thin Solid Films. 520 (2012) 6124–6129. https://doi.org/10.1016/j.tsf.2012.05.086.
[22] R.M. Bowman, J.M. Gregg, VO2 thin films: growth and the effect of applied strain on their resistance, (n.d.) 5.
[23] A.L. Patterson, The Scherrer Formula for X-Ray Particle Size Determination, Phys. Rev. 56 (1939) 978–982. https://doi.org/10.1103/PhysRev.56.978.
[24] B. Zhuang, Z. Dai, S. Pang, H. Xu, L. Sun, F. Ma, 3D Ordered Macroporous VO2 Thin Films with an Efficient Thermochromic Modulation Capability for Advanced Smart Windows, Advanced Optical Materials. 7 (2019) 1900600. https://doi.org/10.1002/adom.201900600.
[25] P. Shvets, O. Dikaya, K. Maksimova, A. Goikhman, A review of Raman spectroscopy of vanadium oxides, Journal of Raman Spectroscopy. 50 (2019) 1226–1244. https://doi.org/10.1002/jrs.5616.
[26] P. Shvets, K. Maksimova, A. Goikhman, Correlation between Raman spectra and oxygen content in amorphous vanadium oxides, Physica B: Condensed Matter. 613 (2021) 412995. https://doi.org/10.1016/j.physb.2021.412995.
[27] J.C. Parker, Raman scattering from VO_{2} single crystals: A study of the effects of surface oxidation, (n.d.) 3.
[28] P. Schilbe, Raman scattering in VO2, Physica B: Condensed Matter. 316–317 (2002) 600–602. https://doi.org/10.1016/S0921-4526(02)00584-7.
[29] I.G. Madiba, N. Émond, M. Chaker, F.T. Thema, S.I. Tadadjeu, U. Muller, P. Zolliker, A. Braun, L. Kotsedi, M. Maaza, Effects of gamma irradiations on reactive pulsed laser deposited vanadium dioxide thin films, Applied Surface Science. 411 (2017) 271–278. https://doi.org/10.1016/j.apsusc.2017.03.131.
[30] J.M. Atkin, S. Berweger, E.K. Chavez, M.B. Raschke, J. Cao, W. Fan, J. Wu, Strain and temperature dependence of the insulating phases of VO${}_{2}$ near the metal-insulator transition, Phys. Rev. B. 85 (2012) 020101. https://doi.org/10.1103/PhysRevB.85.020101.
[31] S.S. Maklakov, V.I. Polozov, S.A. Maklakov, A.D. Mishin, I.A. Ryzhikov, A.L. Trigub, V.A. Amelichev, K.I. Maslakov, V.N. Kisel, Post-deposition annealing of thin RF magnetron sputter-deposited VO2 films above the melting point, Journal of Alloys and Compounds. 763 (2018) 558–569. https://doi.org/10.1016/j.jallcom.2018.06.014.
[32] I.H. Campbell, P.M. Fauchet, The effects of microcrystal size and shape on the one phonon Raman spectra of crystalline semiconductors, Solid State Communications. 58 (1986) 739–741. https://doi.org/10.1016/0038-1098(86)90513-2.
[33] A.K. Arora, M. Rajalakshmi, T.R. Ravindran, V. Sivasubramanian, Raman spectroscopy of optical phonon confinement in nanostructured materials, Journal of Raman Spectroscopy. 38 (2007) 604–617. https://doi.org/10.1002/jrs.1684.
[34] D. Fu, K. Liu, T. Tao, K. Lo, C. Cheng, B. Liu, R. Zhang, H.A. Bechtel, J. Wu, Comprehensive study of the metal-insulator transition in pulsed laser deposited epitaxial VO2 thin films, Journal of Applied Physics. 113 (2013) 043707. https://doi.org/10.1063/1.4788804.
[35] P. Jin, K. Yoshimura, S. Tanemura, Dependence of microstructure and thermochromism on substrate temperature for sputter-deposited VO2 epitaxial films, Journal of Vacuum Science & Technology A. 15 (1997) 1113–1117. https://doi.org/10.1116/1.580439.
[36] L. Fan, X. Wang, F. Wang, Q. Zhang, L. Zhu, Q. Meng, B. Wang, Z. Zhang, C. Zou, Revealing the role of oxygen vacancies on the phase transition of VO 2 film from the optical-constant measurements, RSC Advances. 8 (2018) 19151–19156. https://doi.org/10.1039/C8RA03292K.

[37] J. Zhang, Z. Zhao, J. Li, H. Jin, F. Rehman, P. Chen, Y. Jiang, C. Chen, M. Cao, Y. Zhao, Evolution of Structural and Electrical Properties of Oxygen-Deficient VO2 under Low Temperature Heating Process, ACS Appl. Mater. Interfaces. 9 (2017) 27135–27141. https://doi.org/10.1021/acsami.7b05792.
[38] V.A. Klimov, I.O. Timofeeva, S.D. Khanin, E.B. Shadrin, A.V. Ilinskii, F. Silva-Andrade, Hysteresis loop construction for the metal-semiconductor phase transition in vanadium dioxide films, Tech. Phys. 47 (2002) 1134–1139. https://doi.org/10.1134/1.1508078.
[39] A.M. Makarevich, I.I. Sadykov, D.I. Sharovarov, V.A. Amelichev, A.A. Adamenkov, D.M. Tsymbarenko, A.V. Plokhih, M.N. Esaulkov, P.M. Solyankin, A.R. Kaul, Chemical synthesis of high quality epitaxial vanadium dioxide films with sharp electrical and optical switch properties, J. Mater. Chem. C. 3 (2015) 9197–9205. https://doi.org/10.1039/C5TC01811K.
[40] C. Zhang, C. Koughia, O. Güneş, J. Luo, N. Hossain, Y. Li, X. Cui, S.-J. Wen, R. Wong, Q. Yang, S. Kasap, Synthesis, structure and optical properties of high-quality VO2 thin films grown on silicon, quartz and sapphire substrates by high temperature magnetron sputtering: Properties through the transition temperature, Journal of Alloys and Compounds. 848 (2020) 156323. https://doi.org/10.1016/j.jallcom.2020.156323.
[41] M. Currie, M.A. Mastro, V.D. Wheeler, Characterizing the tunable refractive index of vanadium dioxide, Opt. Mater. Express, OME. 7 (2017) 1697–1707. https://doi.org/10.1364/OME.7.001697.
[42] H. Kakiuchida, P. Jin, S. Nakao, M. Tazawa, Optical Properties of Vanadium Dioxide Film during Semiconductive–Metallic Phase Transition, Jpn. J. Appl. Phys. 46 (2007) L113. https://doi.org/10.1143/JJAP.46.L113.
[43] J.B. Kana Kana, J.M. Ndjaka, G. Vignaud, A. Gibaud, M. Maaza, Thermally tunable optical constants of vanadium dioxide thin films measured by spectroscopic ellipsometry, Optics Communications. 284 (2011) 807–812. https://doi.org/10.1016/j.optcom.2010.10.009.
[44] M. Nagashima, H. Wada, Near infrared optical properties of laser ablated VO2 thin films by ellipsometry, Thin Solid Films. 312 (1998) 61–65. https://doi.org/10.1016/S0040-6090(97)00360-X.
[45] J.B. Kana Kana, J.M. Ndjaka, B.D. Ngom, A.Y. Fasasi, O. Nemraoui, R. Nemutudi, D. Knoesen, M. Maaza, High substrate temperature induced anomalous phase transition temperature shift in sputtered VO2 thin films, Optical Materials. 32 (2010) 739–742. https://doi.org/10.1016/j.optmat.2010.02.005.
[46] Sangappa, S. Asha, T. Demappa, G. Sanjeev, P. Parameswara, R. Somashekar, Spectroscopic and thermal studies of 8MeV electron beam irradiated HPMC films, Nuclear Instruments and Methods in Physics Research Section B: Beam Interactions with Materials and Atoms. 267 (2009) 2385–2389. https://doi.org/10.1016/j.nimb.2009.04.007.
[47] M. Zhou, J. Bao, M. Tao, R. Zhu, Y. Lin, X. Zhang, Y. Xie, Periodic porous thermochromic VO2(M) films with enhanced visible transmittance, Chem. Commun. 49 (2013) 6021–6023. https://doi.org/10.1039/C3CC42112K.
[48] N.A. BAKR, A.M. FUNDE, V.S. WAMAN, M.M. KAMBLE, R.R. HAWALDAR, D.P. AMALNERKAR, S.W. GOSAVI, S.R. JADKAR, Determination of the optical parameters of a-Si:H thin films deposited by hot wire–chemical vapour deposition technique using transmission spectrum only, Pramana - J Phys. 76 (2011) 519–531. https://doi.org/10.1007/s12043-011-0024-4.

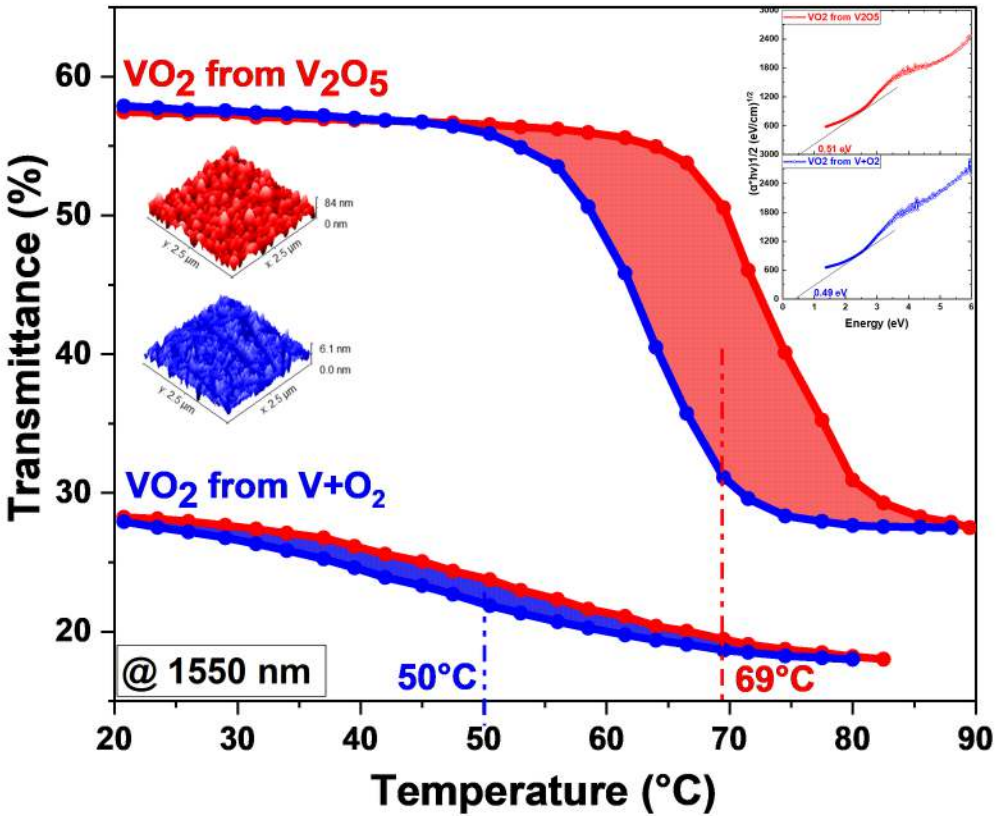
VO2 from V2O5
VO2 from V+O2
@ 1550 nm
50°C
69°C
Transmittance (%)
Temperature (°C)
84 nm
0 nm
6.1 nm
0.0 nm
0.51 eV
0.49 eV
Energy (eV)